Cellulose (2021) 28:10765–10776
https://doi.org/10.1007/s10570-021-04204-y

ORIGINAL RESEARCH

Deswelling of microfibril bundles in drying wood studied by small-angle neutron scattering and molecular dynamics

Aleksi Zitting · Antti Paajanen · Lauri Rautkari · Paavo A. Penttilä

Received: 2 July 2021 / Accepted: 14 September 2021 / Published online: 26 September 2021

Abstract Structural changes of cellulose microfibrils and microfibril bundles in unmodified spruce cell wall due to drying in air were investigated using time-resolved small-angle neutron scattering (SANS). The scattering analysis was supported with dynamic vapor sorption (DVS) measurements to quantify the macroscopic drying kinetics. Molecular dynamics (MD) simulations were carried out to aid in understanding the molecular-level wood-water interactions during drying. Both SANS experiments and simulations support the notion that individual cellulose microfibrils remain relatively unaffected by drying. There is, however, a significant decrease in fibril-to-fibril distances in microfibril bundles. Both scattering and DVS experiments showed two distinct drying regions: constant-rate drying and falling-rate drying. This was also supported by the MD simulation results. The shrinking of the fibril bundles starts at the boundary of these two regions, which is accompanied by a strong decrease in the diffusivity of water in between the microfibrils.

Supplementary Information The online version contains supplementary material available at https://doi.org/10.1007/s10570-021-04204-y.

A. Zitting (✉) · L. Rautkari · P. A. Penttilä
Department of Bioproducts and Biosystems, Aalto University, Espoo, Finland
e-mail: aleksi.zitting@aalto.fi

A. Paajanen
VTT Technical Research Centre of Finland Ltd, Espoo, Finland

Graphic abstract

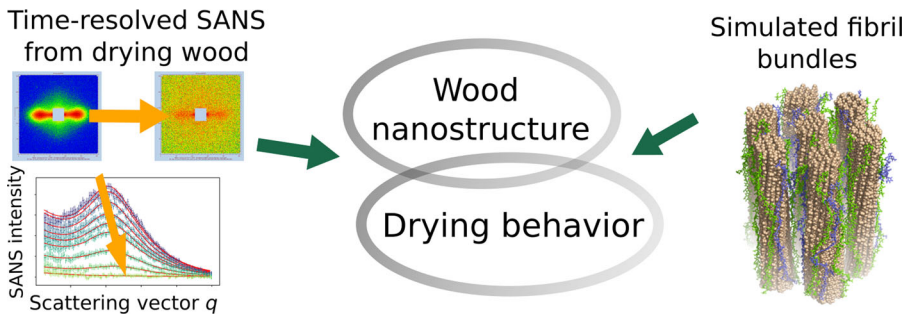

Keywords Wood · Cellulose microfibril · Neutron scattering · Molecular dynamics · Drying kinetics · Moisture behavior

Introduction

Wood-water interactions are one of the most important factors in many use-cases of wood and in the production of advanced bio-based materials from it. These interactions ultimately derive from the nanoscale structure of wood cell wall components interacting with water molecules. However, the exact structure of the cell wall components remains uncertain due to difficulties in imaging them while the cell is still intact.

The relationship between wood moisture content (MC) and fundamental nanoscale structural changes is not yet completely understood (Penttilä et al. 2021). Water inside wood is currently thought to consist of free water inside cell lumina and bound water inside cell walls. When the drying of wood happens sufficiently slowly, it starts with the removal of free water and only then continues onto bound water. However, when the drying rate is fast, both free water and bound water can be simultaneously removed from a sample, until no more free water is left (Penvern et al. 2020).

Small-angle scattering is a non-destructive method for characterizing the average nanostructure of wood cell walls and especially the structures formed by semi-crystalline cellulose microfibrils (diameter 2–3 nm). Small-angle scattering also requires very little sample preparation compared to other methods. Often cutting a small piece of material is enough. This means the wood remains very close to its normal state.

Analysis of wood and its components under various MCs using small-angle scattering is by no means new (Jakob et al. 1996; Penttilä et al. 2021). However, time-resolved measurements remain unexplored, especially with neutron scattering methods. This is due to the time required to gather enough scattering data in a measurement making exploring short time-scale behavior difficult. Modern neutron sources (Lindner and Schweins 2010) allow for high fluxes to be generated and measured in a short amount of time, leading to much faster gathering of good experimental scattering data. Larger and more sensitive detectors allow for high resolution measurements at various length scales.

In this paper, we explore the changes inside the wood cell wall during the drying of never-dried spruce wood utilizing small-angle neutron scattering (SANS). The experimental analysis is supported using molecular simulations of cellulose microfibril bundles (Paajanen et al. 2019), redesigned according to recent information on the molecular architecture of spruce secondary walls (Terrett et al. 2019). By comparing the structural changes in a simulated environment to those determined by experimental means, additional insight can be provided into how water interacts with the structure of the wood cell wall (Penttilä et al. 2021).

Experimental

Sample preparation

Never-dried mature Norway spruce (*Picea abies*) containing both earlywood and latewood was cut into radial longitudinal sections of the dimensions $0.8 \times 10 \times 13$ mm^3 using a sliding microtome. The samples were then stored in plastic vials filled with D_2O for several weeks.

Small-angle neutron scattering

Neutron scattering measurement. Before the measurement the sample was removed from the D_2O vial, visible excess water on the surface was wiped off and the sample was then weighed. The wood sample was inserted partially from one end (a few millimeters) to a glass cuvette to fix its position during the measurement, leaving most of the sample directly exposed to the ambient air of the experimental hall. The ambient temperature and moisture conditions were checked before and after the measurement using an on-site hygro thermometer (RS PRO RS1364 Handheld Hygrometer). The temperature was 24.0°C at the start of the measurement and 23.9°C at the end. The relative humidity (RH) of the air was 25.7% at the start and 25.6% at the end. The beamline also measured the temperature during the experiment which remained at a stable 24°C with very little deviation. The RH could not be measured during the experiment, however any significant changes in humidity seem unlikely.

The quartz cell containing the partially exposed sample was placed in the D11 beamline of Institut Laue–Langevin (ILL). Neutron wavelength used was $\lambda = 6$ Å with the distance to the detector being 1.5 m, with two additional measurements at 8 m at the start and end of the experiment. The neutron beam size was 7 (width) × 10 (height) mm^2. The q-range covered was 0.05–0.33 Å^{-1} at 1.5 m and 0.008–0.06 Å^{-1} at 8 m. After the measurement the sample was weighed again while at equilibrium with ambient air conditions and then dried in an oven for 40 minutes at 105°C to determine the dry weight. For each data point transmission at 8 m sample-to-detector distance was measured 5 minutes before the actual measurement, except for the second data point, where the transmission measurement happened 11 minutes before the measurement.

Data treatment. The SANS data was corrected and normalized to absolute scale using LAMP (Richard et al. 1996) and utilizing the transmission measured at each data point. The equatorial scattering intensity profile was calculated by integrating symmetric 40-degree-wide equatorial sectors. In order to remove the isotropic scattering from the anisotropic scattering of cellulose fibrils, the same symmetric azimuthal integration was done for 80-degree-wide meridional sectors and then the isotropic scattering was subtracted from the equatorial scattering. This integration was done utilizing the pyFAI Python package (Ashiotis et al. 2015).

Model fitting. The corrected and azimuthally integrated small-angle scattering patterns were fitted to the WoodSAS model developed by Penttilä (Penttilä et al. 2019):

$$\begin{aligned} I(q) =& A I_{\mathrm{cyl}}(q, R, \Delta R, a, \Delta a) \\ &+ B_{\mathrm{gauss}} e^{\frac{-q^2}{2\sigma^2}} + C_{\mathrm{porod}} q^{-\alpha} \end{aligned} \tag{1}$$

where A, B_{gauss}, C_{porod}, σ and α are constants. The $I_{\mathrm{cyl}}(q)$ term represents scattering from a hexagonal lattice of infinitely long cylinders, which is a mathematically simple approximation for cellulose microfibrils with R being the mean cylinder radius, a being the center-to-center distance between two adjacent cylinders and ΔR and Δa describe the polydispersity of R and a. The latter two terms represent scattering from larger structures such as microfibril bundles (B_{gauss}-term) and lumina (C_{porod}-term) (Penttilä et al. 2020b). The model fitting was done using the SasView software (Doucet et al. 2018).

Dynamic vapor sorption

To aid with determining the actual MC of the sample during the scattering measurement, additional dynamic vapor sorption (DVS) measurements were performed on separate but similarly sized never-dried spruce samples using a DVS apparatus (DVS Elevated Temperature ET, Surface Measurement Systems Ltd., London, UK). Similar to the scattering experiment, excess moisture was wiped from the surface and the samples were placed inside the DVS sample chamber. The DVS environment was setup to match the experimental conditions with a temperature of 24°C

and RH of 25.5% at the end. The mass of the samples was measured for 12 hours after which the temperature was raised to 60°C and the RH was set to 0% for 6 hours to dry the samples. After drying, the sample was left to equilibrate at temperature of 24°C, RH 0% for several hours to get an accurate dry mass in order to determine the MC of the wood. The MC was defined as follows:

$$MC = \frac{m_{\text{water}}}{m_{\text{dry}}} = \frac{m_{\text{total}} - m_{\text{dry}}}{m_{\text{dry}}} \quad (2)$$

Three separate measurements were performed on samples stored in D_2O. An additional two measurements were performed on samples stored in H_2O to determine if a measurable difference existed between the drying of wood containing D_2O compared to wood containing H_2O. However, no significant difference was found between D_2O and H_2O.

Molecular models

General description of the models and simulations. Molecular models of cellulose microfibril bundles were used for two purposes: (1) to visualize changes in fibril spacing, and (2) to study changes in water mobility due to a changing MC. The former was addressed using a model of seven fibrils that form a close-packed aggregate (non-periodic model), and the latter using a periodic model of four fibrils in a hexagonal lattice (periodic model). In both models, the basic structural unit is a cellulose microfibril segment with adsorbed hemicelluloses.

The microfibrils consist of 18 cellulose chains arranged in the 2-3-4-4-3-2 stacking (Yang and Kubicki 2020). Their internal structure is that of the cellulose I_β polymorph (Nishiyama et al. 2002). The cellulose chains of the non-periodic and periodic models consist of 30 and 34 anhydroglucose units, respectively. In the periodic model, the cellulose chains are periodic along their length, and thus represent an infinitely long fibril.

The hemicelluloses are assumed to reside on the fibril surfaces, following the conceptual model given in Terrett et al. (2019). The hemicelluloses consist of galactoglucomannan (GGM) and glucuronoarabinoxylan (GAX) chains of 30 repeat units. The mass ratio of hemicelluloses to cellulose is roughly 1:4, and that of GGM to GAX is roughly 2:1, both representative of conifer secondary cell walls (Scheller and Ulvskov 2010). The chemical structures correspond to those of spruce hemicelluloses.

Molecular dynamics (MD) simulations were used to create the non-periodic and periodic bundle models. In the first stage, hemicellulose adsorption onto a single microfibril was simulated for eight different hemicellulose configurations. Four GGM chains and two GAX chains with different side group configurations were uniformly distributed around a microfibril segment at a distance of roughly 1 nm from the fibril surface. The chains were distributed in random order, and they were initially in the twofold helical screw conformation and parallel to the fibril axis. After this, the polysaccharides were embedded in water. The hemicelluloses were then adsorbed onto the fibril surfaces in a 100 ns simulation in the canonical ensemble, at 300 K temperature.

In the second stage, the hemicellulose-coated fibrils were used to construct the bundle models. In both cases, the fibrils were arranged in a hexagonal lattice. In the non-periodic model (see Fig. 1), seven fibrils were arranged to form a loose cluster with one central fibril and six peripheral ones. The initial interfibril distance was set to 4.5 nm. The fibrils were then aggregated in a 1 ns simulation in the canonical

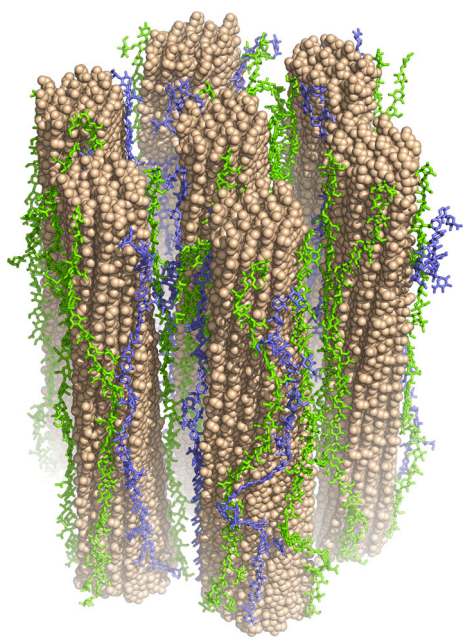

Fig. 1 Non-periodic fibril bundle model consisting of cellulose (beige), GGM (green) and GAX (blue)

ensemble, at 300 K temperature. In the periodic model, four fibrils were arranged to form an infinite hexagonal lattice with an interfibril distance of 5 nm. The interfibrillar cavities were then filled with water to create a system with a MC of roughly 110% $m_{\text{water}}/m_{\text{dry}}$.

Two types of production simulations were carried out. Firstly, the non-periodic bundle was embedded in water, after which water absorption and changes in the bundle geometry were followed in a 600 ns simulation. After this, the water was removed and changes in the bundle geometry were followed in a 100 ns simulation. Secondly, the periodic model was subjected to a drying protocol similar to that used by Kulasinski et al. (2015a). A sequence of 100 ps simulations were carried out, and after each simulation 10 randomly chosen water molecules were removed from the system. Longer 1 ns simulations were carried out at an MC interval of 1 percentage point. The protocol was followed until no water molecules were left in the system. The sequence of bundle structures with different MCs were used as a starting point for 50–200 ns simulations to determine the diffusivity of the inter-fibrillar water. All production simulations were carried out in the isothermal-isobaric ensemble at 300 K temperature and 1 atm external pressure.

Hemicellulose models. The chemical structures used to represent spruce GGM and GAX are based on multiple sources (Terrett et al. 2019; Martínez-Abad et al. 2017; Laine 2005; Willför et al. 2008). The GGM chains have a random backbone of β-(1 → 4)-linked D-glucopyranosyl (Glc*p*) and D-mannopyranosyl (Man*p*) units, with a Glc*p* to Man*p* ratio of 1:4. The Man*p* C2 and C3 hydroxyls are randomly acetylated (Ac), with an Ac to Man*p* ratio of 1:4. The Man*p* units have random α-(1 → 6)-linked D-galactopyranosyl (Gal*p*) side groups, with a Gal*p* to Glc*p* ratio of 1:1.

The GAX chains have a backbone of β-(1 → 4)-linked D-xylopyranosyl (Xyl*p*) units. The Xyl*p* units have a regular pattern of α-(1 → 2)-linked 4-O-methyl glucuronic acid (MeGlcA*p*) side groups, with a MeGlcA*p* attached to every 6th Xyl*p* unit. The MeGlcA*p* to Xyl*p* ratio is thus 1:6. Moreover, there are random α-(1 → 3)-linked L-arabinofuranosyl (Ara*f*) side groups, which only occur two Xyl*p* units removed from the MeGlcA*p* groups towards the non-reducing end of the chain. The Ara*f* to Xyl*p* ratio is 1:12.

Details of the simulation set-up. All simulations were carried out using GROMACS (Abraham et al. 2015). Interatomic forces were described using the GLYCAM06H force field (Kirschner et al. 2008). All bonds involving hydrogen were constrained to a constant bond length using the LINCS method (Hess et al. 1997). The TIP3P model was used to describe water (Jorgensen et al. 1983). Temperature control was realized using a stochastic variant of the Berendsen thermostat (Bussi et al. 2007), and pressure control using the Berendsen barostat (Berendsen et al. 1984). Time constants of 200 fs and 2 ps were used for temperature and pressure control, respectively. The total linear momentum of the system was set to zero at 2 ps intervals. The equations of motion were integrated using the velocity-Verlet algorithm with a 2 fs time step. GROMACS utilities, the Ovito Open Visualization Tool (Stukowski 2009) and MDTraj (McGibbon et al. 2015) were used for trajectory analysis. The doGlycans tool (Danne et al. 2017) was used to generate the molecular structures of the hemicelluloses.

Results and discussion

The neutron scattering from wood generates a scattering pattern based on its inner nanostructure, especially the structure of cellulose microfibrils. By investigating how the scattering data changes with the MC, the changes in the structure of microfibrils and microfibril bundles can be observed. Azimuthal integration of the scattering data yields a peak around $q = 0.16\text{Å}^{-1}$ that corresponds to the microfibril correlation distance. This peak gets smaller and shifts to higher q-values as the sample dries, which is interpreted as a decreased distance between fibrils (Fernandes et al. 2011).

By fitting the integrated scattering data (Fig. 2a) to the model (Eq. 1, "Experimental" section) we get the results shown in Fig. 2b. ΔR was assumed to be 0.2 based on previous scattering experiments (Penttilä et al. 2019), additionally the value does not have a large effect in the measured q-range. The scattering data from beyond 150 minutes was too weak and noisy to provide anything useful due to low contrast between the microfibrils and the dry, compact matrix.

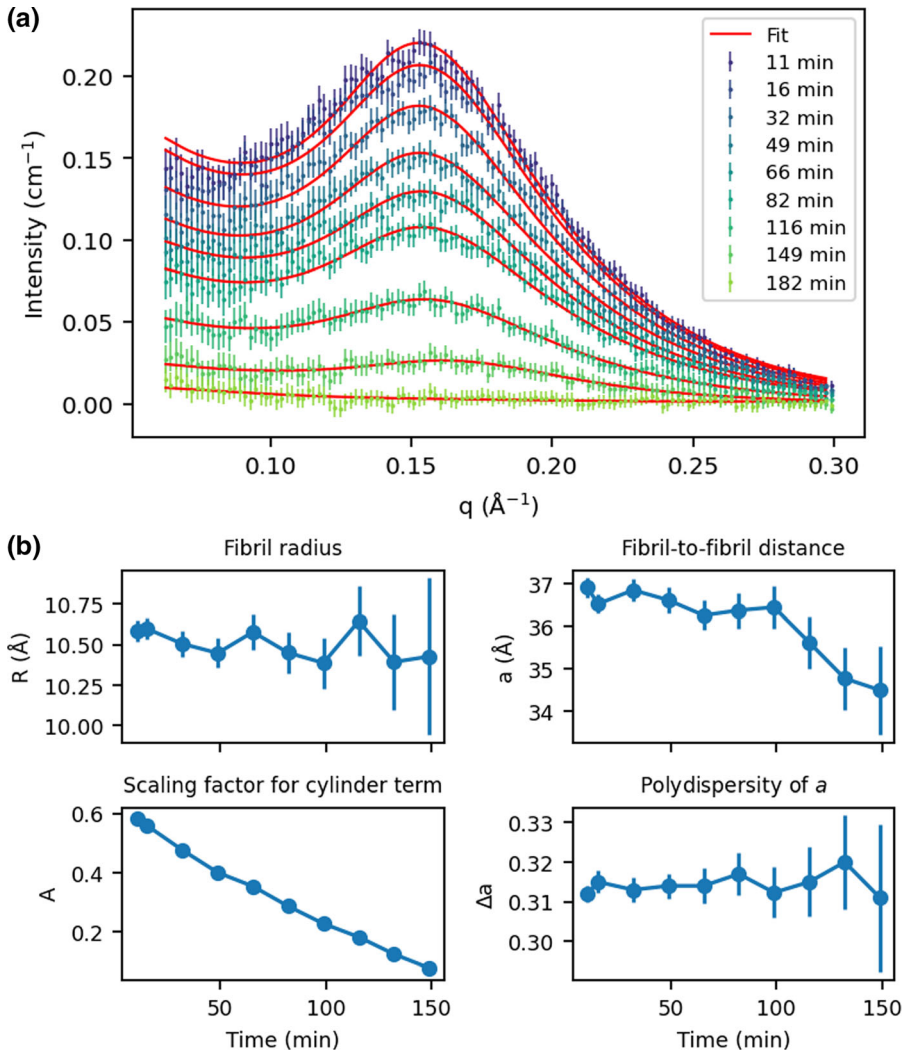

Fig. 2 **a** Fits of the WoodSAS model (Eq. 1) to the integrated equatorial, anisotropic SANS intensity of drying wood **b** The fitted values as a function of time

Both R and Δa are relatively unaffected during the drying. Based on the measured radius, the microfibril diameter is roughly 2.1 nm, which is very similar to other measurements (Fernandes et al. 2011; Penttilä et al. 2019). The center-to-center distance between microfibrils goes from 3.65 (wet) to 3.45 nm (dry) after 140 min. The fibril-to-fibril distance and moisture behavior are roughly similar to those in previous measurements of softwoods (Plaza et al. 2016; Fernandes et al. 2011; Jakob et al. 1996; Penttilä et al. 2019). However, the fibril-to-fibril distance varies typically from 4 nm in the fully wet state to 3 nm in the dry state, which is a more significant change than observed in our current results. This discrepancy may be partly due to uneven drying of the sample, with surfaces drying faster and causing drier regions to lower the value at the start and wet regions to raise it at the end. The sample had also dried slightly before the measurement could be started and was thus not fully wet at the start. Additionally, due to low contrast later on, the value for dry wood could not be accurately measured, and the sample was still above equilibrium MC when the last data point with successfully determined interfibril distance (at 149 min) was measured.

Similar fitting (see Fig. 3) to integrated scattering data was done for two data points measured with a sample-to-detector distance of 8 m. These data points

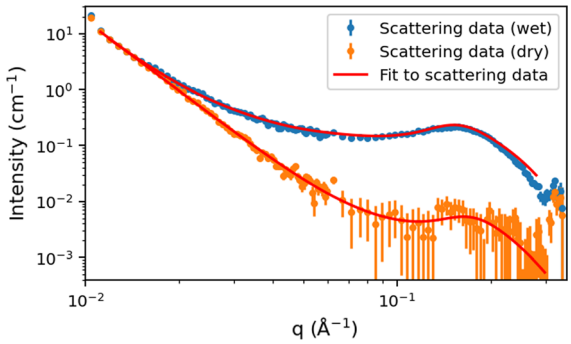

Fig. 3 Equatorial, anisotropic SANS intensities from wet and dry wood, obtained using combined measurements at sample-to-detector distances of 1.5 m and 8 m

were acquired at the beginning of the measurement for wet wood and at the end for dry wood. These were combined with the first and last data points measured at 1.5 m to extend the covered q-range to 0.01–0.3 Å^{-1}. This was done to fit the B_{gauss}-term (Eq. 1, "Experimental" section) to investigate the change in microfibril bundles during drying. Due to poor data for dry wood, any values yielded by the analysis are merely approximate and the values of a and R for dry wood had to be fixed to 34.5 Å and 11 Å respectively, for the fitting to provide meaningful results. Regardless, there was a clear increase in the value of σ from 0.019 to 0.026 Å^{-1}, roughly corresponding to the bundle diameter shrinking from 15 to 11 nm (Penttilä et al. 2020a). While the exact value of the shrinking may not be accurate, evidence for shrinking bundles was still there.

Peak fitting (Fig. 4) was done on the azimuthal SANS scattering profile, in order to determine any changes in the orientational distribution of the microfibrils. A 180-degree-wide equatorial sector was integrated over the q-range 0.12–0.30 Å^{-1} (corresponding to structures between 2 and 5 nm), which corresponds to the level of individual cellulose microfibrils. The peak width remains mostly stable during the drying, possibly decreasing slightly, but data at later times is not accurate enough to say for certain. The mostly unchanging peak width suggests that microfibril angle does not change noticeably during drying, which is consistent with some earlier studies on softwood (Rayirath et al. 2008; Hill et al. 2010). However, this measurement could not accurately probe orientational changes at low MC and other studies have shown both decreasing (Penttilä et al. 2020b) and increasing (Lube et al. 2016) microfibril angles for drying wood. The peak heights show a clear and linear downward trend over the measurement.

While the exact MC of the sample during the scattering measurement was unknown, scattering contrast in the cell wall is proportional to the amount of water remaining among the microfibrils. This means that some scattering terms correlate with the MC of the sample during the measurement. As can be seen in Fig. 5, both the scaling factor A and the azimuthal peak height behaved in a similar manner to the MC of wood measured by DVS. These terms showed similar linear decrease during the first 150 minutes followed by a slow decay towards equilibrium. It stands to reason that these terms can therefore indirectly tell us about the amount of water in the sample, especially at the level of the cellulose microfibrils. The SANS terms have a less steep slope, indicating that the SANS sample dried slower than the DVS samples. This could be due to the experimental setup, since the SANS sample was partially covered by a glass cuvette, reducing the drying surface. The DVS device also had a N_2 flow, slightly accelerating the drying. The relationship between MC and the scaling factor A is further complicated by uneven drying of the sample, which will be discussed later.

The drying kinetics of porous materials has two distinct drying regions, a constant rate period (CRP) where the drying rate of the material remains constant or almost constant. This is followed by a falling rate period (FRP) where the drying rate starts slowing down. Wood is a highly porous material and should therefore exhibit similar behavior (Coumans 2000). Indeed, by looking at the MC and its time derivative as measured by DVS, as seen in Fig. 6, it clearly exhibits constant rate drying until roughly 100 minutes, followed by a falling rate behavior afterwards. At the point where the behavior changes from the CRP-region to FRP-region, at an MC of roughly 60%, the interfibril distance also starts to fall rapidly. After roughly 3 hours, the drying has slowed as the system approaches the equilibrium MC of around 7%, which is consistent with previous results for spruce at 25% RH (Fredriksson and Thybring 2018).

The results are consistent with the interpretation that during CRP-drying, the water is largely removed from the cell lumina. Additionally, some water is

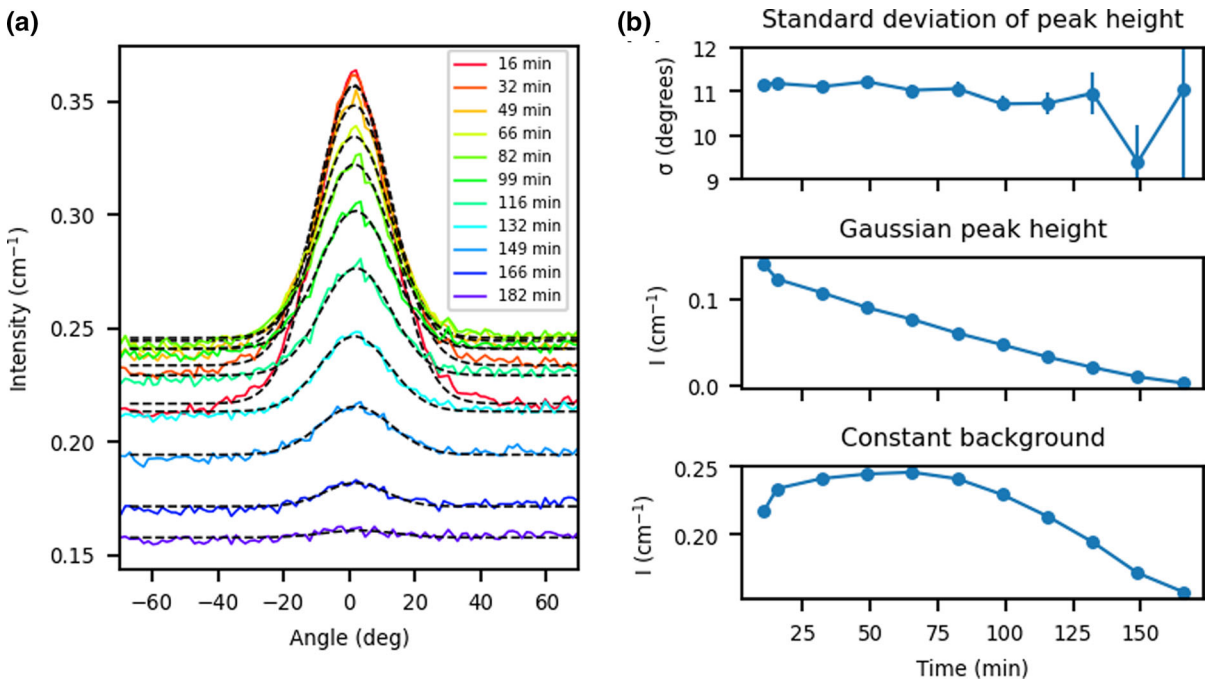

Fig. 4 **a** Gaussian peaks (dashed lines) fitted to the azimuthal SANS intensity profile (solid lines) of drying wood, radially averaged over the q-range 0.12–0.30 $Å^{-1}$ **b** The time evolution of the fitted values

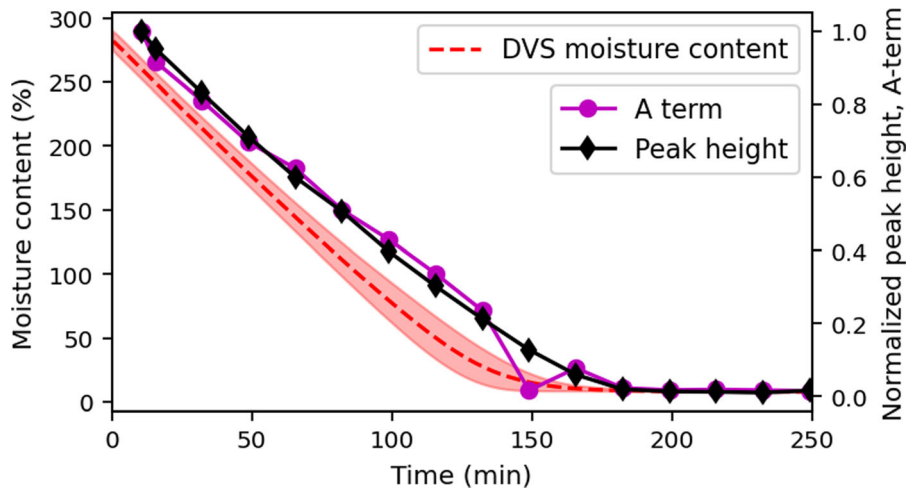

Fig. 5 Moisture content as a function of time measured by DVS and the normalized height of the azimuthal peak and A-term from the WoodSAS model (Eq. 2) as determined by SANS

being lost from inside the cell walls, as can be inferred from the decreasing A-term and Gaussian peak heights seen in Fig. 5. The most likely cause for this initial decrease is the surface drying more quickly than the bulk. As SANS measures the average over the entire neutron interaction volume, this water loss does not substantially affect the fibril-to-fibril distance. Once the FRP-drying begins, the removal of bound water from inside the cell walls starts to dominate the drying and the fibrils start to get closer as water is removed from between them. This FRP-behavior seems to happen at an MC value larger than even the most liberal estimates of wood fibre saturation point (FSP), which is a value at which the cell wall is fully saturated

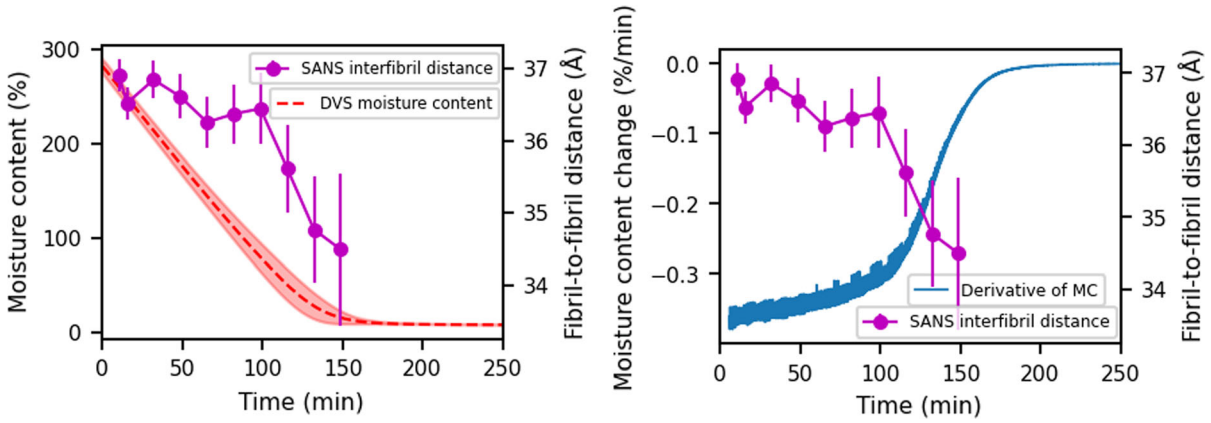

Fig. 6 Fibril-to-fibril distance compared to moisture content measured using DVS (left) and the time-derivative of moisture content (right)

while the lumina are empty (Thybring et al. 2020). However, FSP is a theoretical value usually measured at equilibrium, while the spruce sample measured is a macroscopic object and the drying rate is so fast that the system is nowhere near equilibrium. In addition to the faster drying of surfaces, the volume interacting with the neutron beam contains both earlywood and latewood, which have different lumen sizes and cell wall volume fractions. This means that the MC of the interaction volume will be inhomogeneous. Therefore, even while the average MC of the sample is higher than the FSP, some volume fraction of the sample may be near or below FSP, leading to a decrease in fibril-to-fibril distance.

The fundamental moisture-related changes in the microfibril bundles can be visualized with the aid of atomistic simulations as presented in Fig. 7. When the MC in the simulated model system increases, the water molecules go between the individual fibrils in the bundle and cause the fibrils to drift apart as the water takes up more and more space between them. An equivalent but opposite change happens during drying. The changes to the structure of single fibrils are minor due to water's inability to penetrate into the fibrils. On the contrary, fibril-to-fibril distance noticeably decreases during drying, which agrees with the SANS measurements. Two separate and distinct methods of SANS and atomistic models provide similar values of fibril-to-fibril distances and a similar moisture

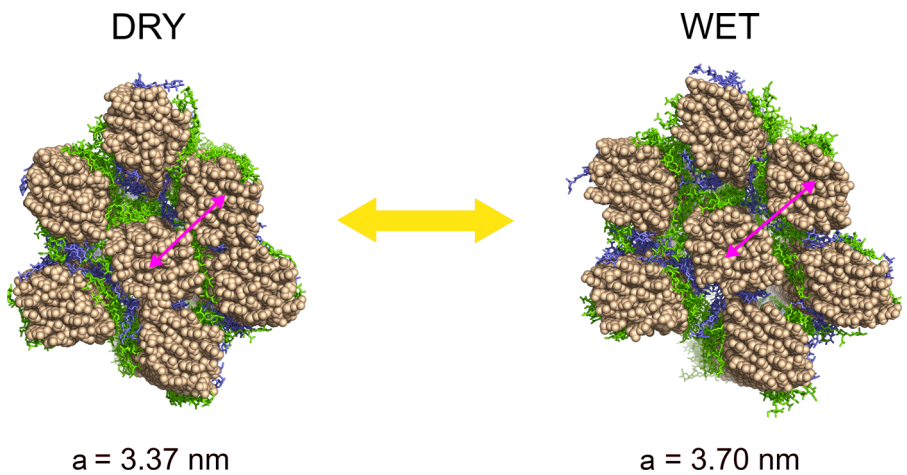

Fig. 7 The non-periodic atomistic model illustrates the change in interfibril distance *a* with changing moisture content. Cellulose fibrils (beige) surrounded by hemicellulose (green/blue) are farther apart when surrounded by water molecules (not shown)

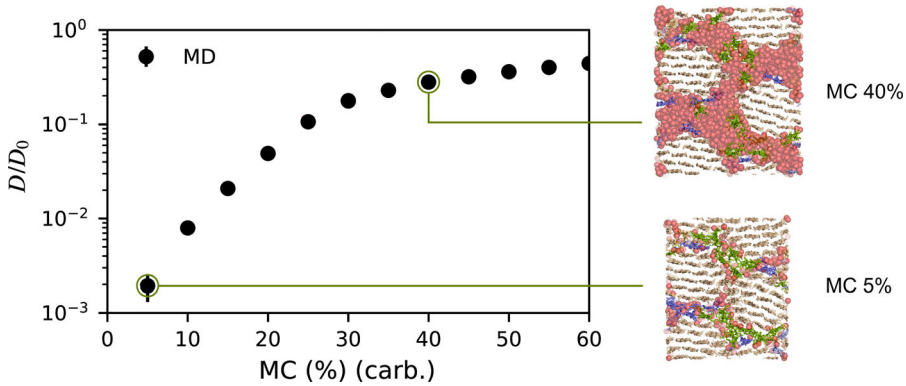

Fig. 8 Diffusivity of water as a function of carbohydrate-based moisture content in the periodic atomistic model. D is the diffusion coefficient of water within the bundle and D_0 is the self-diffusion coefficient

response. This suggests that both methods and their assumptions are valid, and they provide useful tools for characterizing moisture induced changes inside the wood cell wall.

Changes in the diffusivity of water as a function of MC were studied with MD simulations of periodic microfibril bundles. In Fig. 8, the simulated water diffusivity determined using the mean squared displacement of the water molecules is compared to bulk water diffusivity.

The diffusivity remains somewhat stable above MC values of 40% but starts to greatly decrease at around 30% MC. At this point, the amount of water able to freely move compared to water bound to cellulose and hemicelluloses starts to decrease rapidly. This leads to a much lower diffusion coefficient due to decreased water molecule mobility. Similar behavior has been observed before in simulations of crystalline cellulose surrounded by hemicelluloses (Kulasinski et al. 2015a, b) and its relation to fibril-to-fibril distance was discussed by Topgaard and Söderman (2001).

The MC values derived from the models are not directly comparable to experimental values as the model only contains carbohydrate molecules and the water molecules surrounding them, while in the experiments the MC was determined from a macroscopic piece of wood. Additionally, with the periodic model, the change in fibril-to-fibril distance was from 38 to 32 Å while the MC changed from 40 to 5%, which is a noticeably larger change than during the current SANS measurements of drying wood. This could however be explained by the small and constrained periodic structure that allows more efficient packing of the fibrils than possible in a non-periodic system. Regardless, both experimental and simulation results suggest similar behavior due to moisture changes. Both the models and SANS measurements show decreasing fibril-to-fibril distance as the system dries with minimal changes to individual microfibrils. Both also exhibit a period of near constant-rate drying kinetics at high MC, followed by a falling-rate at lower MC.

Conclusions

SANS is a valid method for measuring dynamic moisture related changes inside the wood cell wall.

The changes in the center-to-center distance between microfibrils could be measured while the sample dried in air until the scattering signal got too weak after 150 minutes. Based on both the SANS measurements and the simulations of cellulose microfibril bundles including hemicelluloses, the drying dynamics of spruce wood consisted of two separate regions. Firstly, the constant rate drying, where water loss was almost constant as water primarily left the cell lumina and the cell wall nanostructure remained mostly unaffected. Lastly, the falling rate period, where the cell walls started losing enough moisture to cause the fibrils to get closer to each other as water was lost from between them. During this later period, the diffusion of water slowed down as the fibrils got closer to each other.

Acknowledgments This work was a part of the Academy of Finland's Flagship Programme, under Projects No. 318890 and 318891 (Competence Center for Materials Bioeconomy,

FinnCERES). P.A.P. thanks the Academy of Finland for funding (Grant No. 315768). Institut Laue-Langevin (ILL) (instrument D11, proposal DIR-175) is thanked for provision of facilities and technical assistance. The authors wish to acknowledge CSC – IT Center for Science, Finland, for computational resources. Dr. Ralf Schweins is thanked for assistance with the neutron experiments. Dr. Jukka Ketoja is thanked for valuable discussions.

Author contributions AZ planned the study together with PAP and AP, conducted all data analysis, conducted the DVS measurements, and wrote most of the manuscript. AP created the MD models, conducted the simulations, created model visualizations, and wrote the corresponding experimental section. AZ and PAP designed and conducted the SANS experiments together. PAP prepared the samples and supervised the work. All authors were involved in the interpretation of the results and commented the manuscript draft.

Funding Open access funding provided by Aalto University. This work received funding from the Academy of Finland (Grant No. 315768) and FinnCERES Flagship Programme of the Academy of Finland (Projects No. 318890 and 318891).

Availability of data The neutron scattering and DVS data are available as Supporting Information.

Code availibility The code is available upon reasonable request.

Declarations

Conflict of interest The authors declare that they have no conflict of interest.

Ethical approval No results of studies involving humans or animals are reported.

Consent to participate No results of studies involving humans or animals are reported.

Consent for publication No results of studies involving humans or animals are reported.

References

Abraham MJ, Murtola T, Schulz R, Páll S, Smith JC, Hess B, Lindahl E (2015) GROMACS: high performance molecular simulations through multi-level parallelism from laptops to supercomputers. SoftwareX 1–2:19–25. https://doi.org/10.1016/j.softx.2015.06.001

Ashiotis G, Deschildre A, Nawaz Z, Wright JP, Karkoulis D, Picca FE, Kieffer J (2015) The fast azimuthal integration Python library: pyFAI. J Appl Crystallogr 48(2):510–519. https://doi.org/10.1107/S1600576715004306

Berendsen HJC, Postma JPM, van Gunsteren WF, DiNola A, Haak JR (1984) Molecular dynamics with coupling to an external bath. J Chem Phys 81(8):3684–3690. https://doi.org/10.1063/1.448118

Bussi G, Donadio D, Parrinello M (2007) Canonical sampling through velocity rescaling. J Chem Phys 126(1):014101. https://doi.org/10.1063/1.2408420

Coumans W (2000) Models for drying kinetics based on drying curves of slabs. Chem Eng Process 39(1):53–68. https://doi.org/10.1016/S0255-2701(99)00084-7

Danne R, Poojari C, Martinez-Seara H, Rissanen S, Lolicato F, Róg T, Vattulainen I (2017) doGlycans-tools for preparing carbohydrate structures for atomistic simulations of glycoproteins, glycolipids, and carbohydrate polymers for GROMACS. J Chem Inf Model 57(10):2401–2406. https://doi.org/10.1021/acs.jcim.7b00237

Doucet M, Cho JH, Alina G, Bakker J, Bouwman W, Butler P, Campbell K, Gonzales M, Heenan R, Jackson A, Juhas P, King S, Kienzle P, Krzywon J, Markvardsen A, Nielsen T, O'Driscoll L, Potrzebowski W, Ferraz Leal R, Richter T, Rozycko P, Snow T, Washington A (2018) SasView version 4.2. https://doi.org/10.5281/zenodo.1412041

Fernandes AN, Thomas LH, Altaner CM, Callow P, Forsyth VT, Apperley DC, Kennedy CJ, Jarvis MC (2011) Nanostructure of cellulose microfibrils in spruce wood. Proc Natl Acad Sci USA 108(47):E1195–E1203. https://doi.org/10.1073/pnas.1108942108

Fredriksson M, Thybring E (2018) Scanning or desorption isotherms? Characterising sorption hysteresis of wood. Cellulose 25:4477–4485. https://doi.org/10.1007/s10570-018-1898-9

Hess B, Bekker H, Berendsen HJC, Fraaije JGEM (1997) LINCS: a linear constraint solver for molecular simulations. J Comput Chem 18(12):1463–1472

Hill SJ, Kirby NM, Mudie ST, Hawley AM, Ingham B, Franich RA, Newman RH (2010) Effect of drying and rewetting of wood on cellulose molecular packing. Holzforschung 64(4):421–427. https://doi.org/10.1515/hf.2010.065

Jakob HF, Tschegg SE, Fratzl P (1996) Hydration dependence of the wood-cell wall structure in *Picea abies*. A small-angle x-ray scattering study. Macromolecules 29(26):8435–8440. https://doi.org/10.1021/ma9605661

Jorgensen WL, Chandrasekhar J, Madura JD, Impey RW, Klein ML (1983) Comparison of simple potential functions for simulating liquid water. J Chem Phys 79(2):926–935. https://doi.org/10.1063/1.445869

Kirschner KN, Yongye AB, Tschampel SM, González-Outeiriño J, Daniels CR, Foley BL, Woods RJ (2008) GLYCAM06: a generalizable biomolecular force field.

carbohydrates. J Comput Chem 29(4):622–655. https://doi.org/10.1002/jcc.20820
Kulasinski K, Guyer R, Derome D, Carmeliet J (2015a) Water adsorption in wood microfibril-hemicellulose system: Role of the crystalline-amorphous interface. Biomacromolecules 16(9):2972–2978. https://doi.org/10.1021/acs.biomac.5b00878
Kulasinski K, Guyer R, Derome D, Carmeliet J (2015b) Water diffusion in amorphous hydrophilic systems: a stop and go process. Langmuir 31(39):10843–10849. https://doi.org/10.1021/acs.langmuir.5b03122
Laine C (2005) Structures of hemicelluloses and pectins in wood and pulp. Doctoral thesis
Lindner P, Schweins R (2010) The D11 small-angle scattering instrument: a new benchmark for SANS. Neutron News 21:15–18. https://doi.org/10.1080/10448631003697985
Lube V, Lazarescu C, Mansfield SD, Avramidis S (2016) Wood microfibril angle variation after drying. Holzforschung 70(5):485–488. https://doi.org/10.1515/hf-2014-0334
Martínez-Abad A, Berglund J, Toriz G, Gatenholm P, Henriksson G, Lindström M, Wohlert J, Vilaplana F (2017) Regular motifs in xylan modulate molecular flexibility and interactions with cellulose surfaces. Plant Physiol 175(4):1579–1592. https://doi.org/10.1104/pp.17.01184
McGibbon RT, Beauchamp KA, Harrigan MP, Klein C, Swails JM, Hernández CX, Schwantes CR, Wang LP, Lane TJ, Pande VS (2015) MDTraj: a modern open library for the analysis of molecular dynamics trajectories. Biophys J 109(8):1528–1532. https://doi.org/10.1016/j.bpj.2015.08.015
Nishiyama Y, Langan P, Chanzy H (2002) Crystal structure and hydrogen-bonding system in cellulose I-beta from synchrotron X-ray and neutron fiber diffraction. J Am Chem Soc 124(31):9074–9082. https://doi.org/10.1021/ja0257319
Paajanen A, Ceccherini S, Maloney T, Ketoja JA (2019) Chirality and bound water in the hierarchical cellulose structure. Cellulose 26(10):5877–5892. https://doi.org/10.1007/s10570-019-02525-7
Penttilä PA, Rautkari L, Österberg M, Schweins R (2019) Small-angle scattering model for efficient characterization of wood nanostructure and moisture behaviour. J Appl Crystallogr 52(2):369–377. https://doi.org/10.1107/S1600576719002012
Penttilä PA, Altgen M, Carl N, van der Linden P, Morfin I, Österberg M, Schweins R, Rautkari L (2020b) Moisture-related changes in the nanostructure of woods studied with X-ray and neutron scattering. Cellulose 27(17):71–87. https://doi.org/10.1007/s10570-019-02781-7
Penttilä PA, Altgen M, Awais M, Österberg M, Rautkari L, Schweins R (2020a) Bundling of cellulose microfibrils in native and polyethylene glycol-containing wood cell walls revealed by small-angle neutron scattering. Sci Rep 10:20844. https://doi.org/10.1038/s41598-020-77755-y
Penttilä PA, Paajanen A, Ketoja JA (2021) Combining scattering analysis and atomistic simulation of wood-water interactions. Carbohydr Polym 251:117064. https://doi.org/10.1016/j.carbpol.2020.117064
Penvern H, Zhou M, Maillet B, Courtier-Murias D, Scheel M, Perrin J, Weitkamp T, Bardet S, Caré S, Coussot P (2020) How bound water regulates wood drying. Phys Rev Appl 14:054051. https://link.aps.org/doi/10.1103/PhysRevApplied.14.054051
Plaza NZ, Pingali SV, Qian S, Heller WT, Jakes JE (2016) Informing the improvement of forest products durability using small angle neutron scattering. Cellulose 23(3):1593–1607. https://doi.org/10.1007/s10570-016-0933-y
Rayirath P, Avramidis S, Mansfield SD (2008) The effect of wood drying on crystallinity and microfibril angle in black spruce (*Picea mariana*). J Wood Chem Technol 28(3):167–179. https://doi.org/10.1080/02773810802346950
Richard D, Ferrand M, Kearley GJ (1996) Analysis and visualisation of neutron-scattering data. J Neutron Res 4:33–39. https://doi.org/10.1080/10238169608200065
Scheller HV, Ulvskov P (2010) Hemicelluloses. Annu Rev Plant Biol 61(1):263–289. https://doi.org/10.1146/annurev-arplant-042809-112315
Stukowski A (2009) Visualization and analysis of atomistic simulation data with OVITO-the open visualization tool. Model Simul Mater Sci Eng 18(1):015012. https://doi.org/10.1088/0965-0393/18/1/015012
Terrett OM, Lyczakowski JJ, Yu L, Iuga D, Franks WT, Brown SP, Dupree R, Dupree P (2019) Molecular architecture of softwood revealed by solid-state NMR. Nat Commun 10(1):4978. https://doi.org/10.1038/s41467-019-12979-9
Thybring EE, Digaitis R, Nord-Larsen T, Beck G, Fredriksson M (2020) How much water can wood cell walls hold? A triangulation approach to determine the maximum cell wall moisture content. PLoS ONE 15(8):1–18. https://doi.org/10.1371/journal.pone.0238319
Topgaard D, Söderman O (2001) Diffusion of water absorbed in cellulose fibers studied with 1H-NMR. Langmuir 17(9):2694–2702. https://doi.org/10.1021/la0009821
Willför S, Sundberg K, Tenkanen M, Holmbom B (2008) Spruce-derived mannans—a potential raw material for hydrocolloids and novel advanced natural materials. Carbohydr Polym 72(2):197–210. https://doi.org/10.1016/j.carbpol.2007.08.006
Yang H, Kubicki JD (2020) A density functional theory study on the shape of the primary cellulose microfibril in plants: effects of C6 exocyclic group conformation and H-bonding. Cellulose 27(5):2389–2402. https://doi.org/10.1007/s10570-020-02970-9